Radiotherapy and Oncology 138 (2019) 141–148

Contents lists available at ScienceDirect

Radiotherapy and Oncology

journal homepage: www.thegreenjournal.com

Original Article

Radiomics analysis of magnetic resonance imaging improves diagnostic performance of lymph node metastasis in patients with cervical cancer

Qingxia Wu [a,b,c,1], Shuo Wang [d,e,f,1], Xi Chen [g,e,1], Yan Wang [a,b,c], Li Dong [h,b,c], Zhenyu Liu [e,f,*], Jie Tian [e,d,i,f,*], Meiyun Wang [a,b,c,*]

[a] Department of Medical Imaging, Henan Provincial People's Hospital, Zhengzhou; [b] Zhengzhou University People's Hospital, Zhengzhou; [c] Henan University People's Hospital, Zhengzhou; [d] Beijing Advanced Innovation Center for Big Data-Based Precision Medicine, School of Medicine, Beihang University, Beijing; [e] Key Laboratory of Molecular Imaging, Institute of Automation, Chinese Academy of Sciences, Beijing; [f] University of Chinese Academy of Sciences, Beijing; [g] School of Information and Electronics, Beijing Institute of Technology, Beijing; [h] Department of Gynaecology, Henan Provincial People's Hospital, Zhengzhou; and [i] Engineering Research Center of Molecular and Neuro Imaging of Ministry of Education, School of Life Science and Technology, Xidian University, Xi'an, Shanxi, China.

ARTICLE INFO

Article history:
Received 10 January 2019
Received in revised form 21 March 2019
Accepted 29 April 2019
Available online 25 June 2019

Keywords:
Radiomics
Cervical cancer
Lymph nodes
Magnetic resonance imaging

ABSTRACT

Background and purpose: Robust parameters are needed to predict lymph node metastasis (LNM) in locally advanced cervical cancer patients in order to select optimal treatment regimen. The aim of this study is to utilize radiomics analysis of magnetic resonance imaging (MRI) to improve diagnostic performance of LNM in cervical cancer patients.

Materials and methods: A total of 189 cervical cancer patients were divided into a training cohort (n = 126) and a validation cohort (n = 63). For each patient, we extracted radiomic features from intratumoral and peritumoral tissues on sagittal T2WI and axial apparent diffusion coefficient (ADC) maps. Afterward, the radiomic features associated with LNM status were selected by univariate ROC testing and logistic regression with the least absolute shrinkage and selection operator (LASSO) penalty in the training cohort. Based on the selected features, a support vector machine (SVM) model was established to predict LNM status. To further improve the diagnostic performance, a decision tree which combines the radiomics model with clinical factors was built.

Results: Radiomics model of the intratumoral and peritumoral tissues on T2WI ($T2_{tumor+peri}$) showed best sensitivity and clinical LN (c-LN) status showed best specificity to predict LNM. The decision tree that combines radiomics model of $T2_{tumor+peri}$ and c-LN status achieved best diagnostic performance, with AUC and sensitivity of 0.895 and 94.3%, 0.847 and 100% in the training and validation cohort respectively.

Conclusions: The decision tree, which incorporates radiomics model of $T2_{tumor+peri}$ and c-LN status can be potentially applied in the preoperative prediction of LNM in locally advanced cervical cancer patients.

The primary treatment for stage Ib-IIa cervical cancer is either surgery or chemoradiotherapy, which have similar survival rates [1]. Complete lymphadenectomy is recommended by the US National Comprehensive Cancer Network (NCCN) for the surgery of cervical cancer patients. Adjuvant chemoradiotherapy is needed if lymph node metastasis (LNM) is detected histopathologically after surgery. Combined surgery and chemoradiotherapy is associated with increased adverse effects and more complications and should be avoided in the treatment plan [1]. Criteria for selecting cervical cancer patients for radical hysterectomy should be defined so that postoperative adjuvant chemoradiotherapy will be given to a maximum of 5% to 20% of the patients [2]. Thus a preoperative and noninvasive test to determine lymph node (LN) status with high diagnostic performance is of great importance to select the most appropriate treatment option and avoid unnecessary surgical intervention for locally advanced cervical cancer patients.

Many attempts have been made to improve the precise LN status evaluation before operation, including magnetic resonance imaging (MRI), positron emission tomography (PET)-computed tomography (CT) and sentinel lymph node (SLN) biopsy, with SLN providing best diagnostic accuracy, followed by PET-CT and MRI [3]. However, unusual lymphatic drainage patterns that exist, the preoperative lymphoscintigraphy, and experience of the surgeons in SLN biopsy influence the SLN biopsy results [4,5]. Although PET-CT is superior to MRI, considering the limited

* Corresponding authors at: 95 Zhongguancun East Road, Beijing 100190, China (Z. Liu and J. Tian). No. 7 Weiwu Road, Zhengzhou, Henan 450003, China (M. Wang).
E-mail addresses: zhenyu.liu@ia.ac.cn (Z. Liu), jie.tian@ia.ac.cn (J. Tian), mywang@ha.edu.cn (M. Wang).
[1] These authors contributed equally to this article.

https://doi.org/10.1016/j.radonc.2019.04.035
0167-8140/

PET-CT facilities and extensive clinical application of MRI for pretherapeutic evaluation of cervical cancer, it is worthwhile to explore parameters of MRI to diagnose LN metastasis (LNM) [6]. Besides, MRI was more sensitive than PET/CT for detecting metastatic LN in patients with cervical cancer [7]. MRI has long been the modalities of choice for the preoperative detection of LNM in patients with cervical cancer according to morphologic criteria such as size and shape. However, these methods cannot help detect small metastatic LN and may be falsely positive in LNs enlarged owing to hyperplasia. Quantitative analysis based on both tumor and LNs resulted in inconsistent results, which may be due to the inferior capability of parameters reflecting tumor heterogeneity and the difficulty in the one-by-one correspondence with image and pathology [8–11].

Radiomics analysis can provide various high-dimensional data that reflect tumor heterogeneity which cannot be identified by general gross observation [12–15]. Radiomics analysis has showed potential in the preoperative evaluation of LN status in colorectal, bladder and breast cancer, with AUC of 0.736–0.926 [16–19].

Primary tumors metastasize through lymphatics to regional LNs [20]. Functional lymphatics is absent in many tumors but can be identified in the tumor margin and peritumoral tissue [21–23]. Active lymphangiogenesis with abnormal function of altered lymph flow can occur in the peritumoral tissue [21] and lymphatics in the tumor margin facilitate lymphatic metastasis [24]. The peritumoral tissue plays an important role in the process of LN metastasis. To the best of our knowledge, there has been no radiomics study for the preoperative prediction of LN metastasis based on cervical cancer and peritumoral tissues.

Hence, in this study, we sought to utilize radiomics analysis of MRI based on both of the intratumoral and peritumoral tissues to improve diagnostic performance for the preoperative prediction of LN metastasis in patients with cervical cancer.

Materials and methods

Patients

Our institutional review board approved this retrospective study and the informed consent from patients were waived.

A total of 189 consecutive patients with cervical cancer who were treated between March 2012 and December 2017 were enrolled in our study, according to the following inclusion criteria: (i) patients who underwent radical hysterectomy and pelvic lymphadenectomy; (ii) All patients who received no treatment before MRI examination; (iii) patients whose MRI including sagittal T2WI and axial DWI was performed fewer than 15 days before surgery. The exclusion criteria were as follows: (i) patients who underwent preoperative therapy (neoadjuvant chemotherapy, radiotherapy, or conization); (ii) lesions invisible on both sagittal T2WI and axial DWI; (iii) poor image quality because of patients' motion during examination and chemical shift artifacts from gas in the colon and rectum; (iv) suffering from other rare types of cervical tumor.

Patients' characteristics including age, menstrual status, International Federation of Gynecology and Obstetrics (FIGO) stage, histopathological features after surgery including tumor type, LN and lymphovascular space invasion (LVSI) status were obtained by reviewing the medical records. All MRI scans were reviewed by two radiologists with 9 and 8 years of experience in pelvic disease interpretation. The maximal tumor diameter (MTD), the short diameter of largest LN in pelvic area were recorded. Based on commonly used criteria in daily clinical practice, patients with the short diameter of largest LN larger than 10 mm were regarded as positive clinical LN (c-LN) status [25]. Any disagreement was resolved by consultation.

MRI acquisition

All patients underwent pelvic MRI using one of the two 3.0-T MR image systems, either with (Discovery MR 750; GE Medical Systems, Milwaukee, Wis) or (Magnetom TrioTim; Siemens Healthineers) equipped with an 8-channel phased-array coil in supine position. Sagittal T2WI (TR/TE: 4000/87 ms; FOV = 320 × 260 mm^2; matrix = 348 × 299; slice thickness/gap: 4/1mm) and Axial DWI (TR/TE: 4616/76 ms; FOV: 300 × 300 mm^2; matrix: 200 × 196; slice thickness/gap: 6/1 mm; b values of 0 and 800 s/mm^2) were obtained using single-shot spin-echo echo-planar imaging (EPI)) were retrieved from the picture archiving and communication system (PACS) for image feature extraction.

Image segmentation

ITK-SNAP software were explored for three-dimensional manual segmentation (open source software; www.itksnap.org). All manual segmentations of the intratumoral and peritumoral tissues on sagittal T2WI and axial DWI were done by a radiologist who had 8 years of experience in gynecological MR imaging, and each segmentation was validated by a senior radiologist, who had 9 years of experience. The peritumoral tissue was defined as 5 pixels larger around the tumor [26]. Apparent diffusion coefficient (ADC) maps were generated using monoexponential model according to the two b values of DWI. Intratumoral and peritumoral tissues were annotated on DWI with b value of 800 s/mm^2 and then copied to the corresponding ADC maps [27]. The radiomics workflow is presented in Fig. 1.

Radiomic feature extraction

After intratumoral and peritumoral tissues were manually segmented, an open-source software named PyRadiomics was used for radiomic feature extraction [28]. T2WI and ADC maps were standardized by z-score normalization to obtain a standard normal distribution of the image intensities. Afterward, we extracted radiomic features of intratumoral and peritumoral tissues on T2WI and ADC maps respectively.

From each of intratumoral and peritumoral tissues on T2WI ($T2_{tumor}$ and $T2_{peri}$), we extracted 1299 radiomic features including (i) 19 intensity features: these features are the first-order statistics calculated from the tumor intensities such as entropy, reflecting the signal intensity for different tumors, (ii) 16 shape features: evaluate the size and shape information of tumor, which are commonly used for identifying LN in clinical, (iii) 74 texture features: these features measure the relationship between each tumor voxel and its surrounding environments, which can quantify intra-tumor heterogeneity and complex tumor patterns such as the use of size-zone matrix [29], (iv) 736 wavelet features: we decomposed the MR image into low and high frequencies and extracted the features in group i and ii from each frequency range. The wavelet transformation enables us to quantify high-dimensional multi-frequency tumor information that are difficult to be visually interpreted, and (v) 460 Laplacian of Gaussian (LoG) features: these are textural features extracted after a Laplacian of Gaussian spatial band-pass filter. These features describe the tumor information from multi-scale space that combines both the very detailed and macroscopic tumor texture patterns. From each of intratumoral and peritumoral tissues on ADC maps (ADC_{tumor} and ADC_{peri}), we extracted the first four groups of features as in the T2WI. The resolution of the ADC maps is lower than that of T2WI. Therefore, we excluded the LoG features for ADC maps since the multi-scale space information contains much noise when the spatial resolution is low. Finally, 1299 radiomic features were extracted for each of the $T2_{tumor}$ and $T2_{peri}$

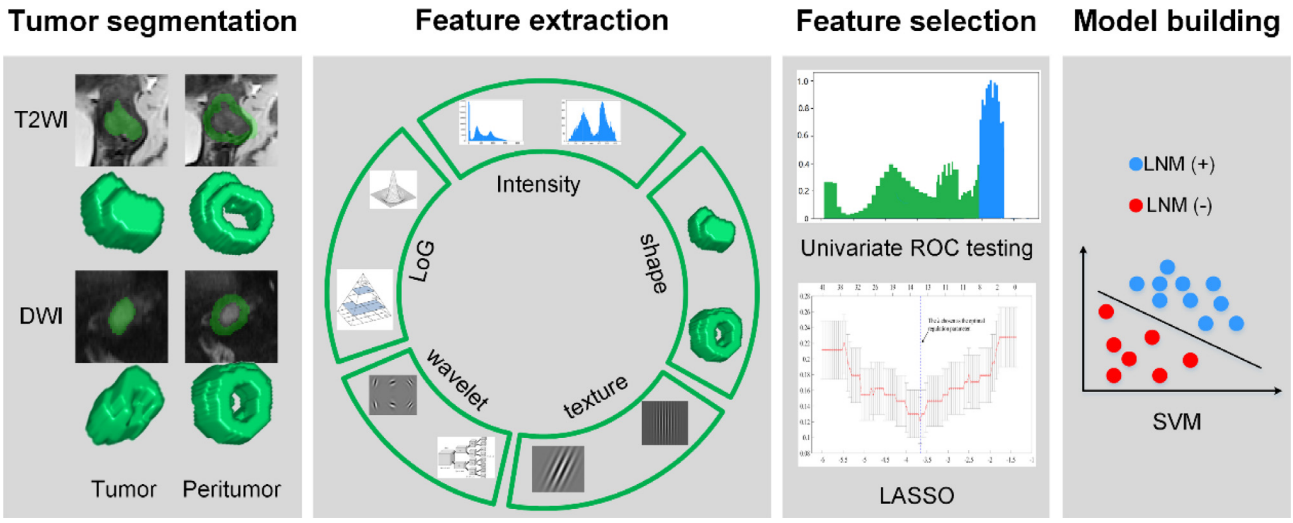

Fig. 1. The radiomics workflow.

areas; and 838 radiomic features were extracted for each of the ADC_{tumor} and ADC_{peri} areas.

Radiomic feature selection

Although the radiomic features reflect tumor information from various perspectives, not all of them are correlated with LNM. Consequently, we used a two-step feature selection to reserve the important features that are highly associated with LNM. First, we examined the univariate predictive performance for all the radiomic features by univariate ROC testing in the training cohort. According to the area under the ROC curve (AUC), the first 20% features with the highest AUC were selected for candidate. Second, we used regularized multivariate logistic regression with the least absolute shrinkage and selection operator (LASSO) penalty for multivariate feature selection. The LASSO regularization involves a parameter λ to control the number of selected features where a larger λ reserves more features. To obtain an optimal feature number and avoid over-fitting, we used 5-fold cross validation in the training cohort to choose the optimal λ. The λ value that maximized the AUC in the training cohort was selected as the optimal regularization parameter, and the feature number was therefore determined automatically by the λ [30].

Radiomics model building

After feature selection, we used a support vector machine (SVM) model to predict the LNM by the selected features. The SVM model used a radial basis kernel and a regularization parameter C. To determine the optimal C value that controls the generalization ability of the SVM model, we used 5-fold cross validation in the training cohort. The C value that maximized the AUC in the training cohort was selected as the optimal regularization parameter. After being trained in the training cohort with the optimal C value, the SVM model predicts a radiomics signature indicating the LNM probability for each patient.

Statistical analysis

All the statistical analyses in this study were implemented with SPSS 21 and python 2.7. The independent sample t test was used to assess the significance of the mean value on age between LNM positive and LNM negative groups. The chi-squared test was used to evaluate the significance of the categorical variables such as menstrual status, FIGO stage, MTD, histology and lymphovascular (LVSI) between LNM positive and LNM negative groups in the training and validation cohorts, respectively. For the variables that have frequency less than 5, the Fisher's exact test was used. P value of less than 0.05 was considered as a significant difference. The logistic regression with LASSO penalty and the SVM model were implemented using python 2.7 in the scikit-learn package.

Results

Demographic and clinical data

Of the 429 patients with cervical cancer scheduled for radical hysterectomy and pelvic lymphadenectomy between March 2012 and December 2017, 145 patients who underwent preoperative neoadjuvant chemotherapy or radiotherapy and 34 patients who underwent preoperative conization were excluded; 40 patients were excluded because of lesions of cervix were invisible on MRI; 11 patients were excluded because of poor image quality either due to motion or chemical shift artifact; and 10 patients were excluded because they suffered from rare tumor type of cervix, including 2 patients with carcinosarcoma, 3 patients with neuroendocrine carcinoma, 1 patient with polypoid adenomyoma, 1 patient with myofibroblastoma, 1 patient with follicular soft tissue sarcoma, 2 patients with small cell tumors; finally, 189 patients fulfilled the eligibility criteria and were enrolled (Fig. 2). All the enrolled patients were sorted in chronological order, the first 2/3 (126 patients between March 2012 and March 2017) constituted the training cohort, and the last 1/3 (63 patients between March 2017 and December 2017) constituted the validation cohort. Patients' Characteristics were given in Table 1.

LNM prevalence was 27.8% and 22.2% in the training and validation cohorts, respectively. Distribution of clinical (patients age, FIGO stage, menstrual status), MTD, c-LN status and pathological characteristics (histology, LVSI) were balanced between the training and validation cohorts. The MTD and c-LN status showed statistical difference between patients with and without LNM both in the training and validation cohorts, as were shown in Table 1.

Feature selection and radiomics model building

The c-LN status showed differential diagnosis of LNM in both the training cohort (AUC = 0.695, accuracy = 82.5%, sensitivity = 40.1% and specificity = 98.8%) and the validation cohort

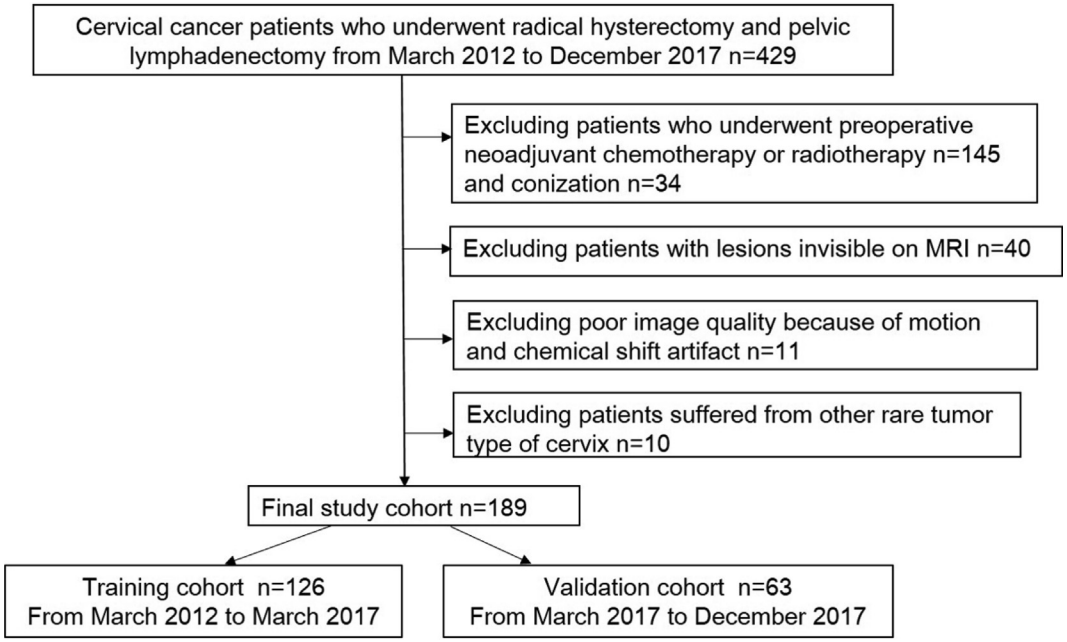

Fig. 2. The patients' recruitment pathway.

Table 1
Characteristics of patients in the training and validation cohorts.

	Training Cohort n = 126			Validation Cohort n = 63			P†
Characteristics	LNM(+) 35(27.8)	LNM(−) 91(72.2)	P	LNM(+) 14(22.2)	LNM(−) 49(77.8)	P	0.411
Age, years			0.634			0.431	0.885
Mean	49	50		48	50		
Range	33–67	27–71		29–67	32–75		
Menstrual status (N. %)			0.421			0.229	0.836
Premenopausal	22(62.9)	50(54.9)		10(71.4)	25(51.0)		
Postmenopausal	13(37.1)	41(45.1)		4(28.6)	24(49.0)		
FIGO Stage (N. %)			0.582			<0.0001	0.280
IB	17(48.6)	38(41.8)		3(21.4)	32(65.3)		
IIA	13(37.1)	43(47.3)		5(35.7)	16(32.7)		
IIB	5(14.3)	10(11.0)		6(42.9)	1(2.0)		
MTD (N. %)			0.001			0.007	0.405
≤4 cm	20(57.1)	77(84.6)		6(42.9)	39(79.6)		
>4 cm	15(42.9)	14(15.4)		8(57.1)	10(20.4)		
c-LN status (N. %)			<0.0001			0.001	0.694
Negative	18(51.4)	85(93.4)		6(42.9)	44(89.8)		
Positive	17(48.6)	6(6.6)		8(57.1)	5(10.2)		
Histology (N. %)			0.603			1.000	0.592
SCC	30(85.7)	77(84.6)		13(92.9)	44(89.8)		
AC	5(14.3)	10(11.0)		1(1.1)	4(8.2)		
ASC	0(0)	4(4.4)		0(0)	1(2.0)		
LVSI (N. %)			<0.0001			0.035	0.148
Negative	11(31.4)	63(69.2)		3(21.4)	27(55.1)		
Positive	24(68.6)	28(30.8)		11(78.6)	22(44.9)		

Note: p is derived from the univariable association analyses of each clinicopathologic variable between patients with and without LNM in the training and validation cohort respectively. p† represents the difference of each clinicopathological variable between the training and validation cohorts.
Abbreviations: LNM: lymph node metastasis; c-LN status: clinical lymph node status; SCC: squamous cell carcinoma; AC: adenocarcinoma; ASC: adenosquamous carcinoma; LVSI: lymphovascular invasion.

(AUC = 0.717, accuracy = 87.4%, sensitivity = 43.1% and specificity = 100%) as shown in the Table 2. Among all the preoperative clinical factors in Table 1, the c-LN status, MTD and FIGO stages showed significant difference ($p < 0.05$) between LNM positive and LNM negative groups in either the training cohort or the validation cohort. Among all the preoperative clinical factors, c-LN status is the best clinical factor for LNM status prediction (Table 2), which is consistent with prior studies [8,17]. The clinical model incorporating c-LN status, MTD and FIGO stages showed similar performance compared with using c-LN status alone in the training cohort (AUC = 0.731, accuracy = 84.2%, sensitivity = 51.5% and specificity = 96.7%) and the validation cohort (AUC = 0.722, accuracy = 85.7%, sensitivity = 57.3% and specificity = 93.9%).

As single layer, radiomics model of intratumoral tissue on ADC maps (ADC_{tumor}) showed best sensitivity in predicting LNM, with 83.1% in the training cohort and 85.6% in the validation cohort; radiomics model of peritumoral tissue on T2WI ($T2_{peri}$) showed high specificity with 97.8% in the training cohort and 95.8% in the validation cohort.

When the intratumoral and peritumoral tissues were combined together, T2WI showed best sensitivity in detecting LNM, with 91.4% and 85.7% in the training and validation cohort respectively.

Table 2
Performance of the clinical model and the radiomics model.

			Training Cohort				Validation Cohort			
			AUC	ACC (%)	SEN (%)	SPE (%)	AUC	ACC (%)	SEN (%)	SPE (%)
Clinical	c-LN		0.695	82.5	40.1	98.8	0.717	87.4	43.1	100
	MTD		0.637	73.0	42.9	84.6	0.684	74.6	57.1	79.6
	FIGO		0.551	51.6	62.9	47.3	0.485	39.7	64.3	32.7
	c-LN+MTD+FIGO		0.731	84.2	51.5	96.7	0.722	85.7	57.3	93.9
Radiomics	Single layer	$T2_{tumor}$	0.870	84.3	77.4	86.9	0.699	73.1	64.6	75.5
		$T2_{peri}$	0.871	80.9	36.9	97.8	0.739	84.1	43.0	95.8
		ADC_{tumor}	0.819	66.7	83.1	60.4	0.750	65.2	85.6	59.3
		ADC_{peri}	0.807	80.9	54.1	91.2	0.628	69.8	49.9	75.5
	Two layers	$T2_{tumor+peri}$	0.975	87.2	91.4	85.7	0.794	73.1	85.7	69.4
		$ADC_{tumor+peri}$	0.890	83.4	57.3	93.4	0.665	71.4	49.4	77.7
Decision tree	$T2_{tumor+peri}$+c-LN		0.895	87.3	94.3	84.6	0.847	76.2	100	69.3

Table 3
Radiomic features for the model of $T2_{tumor+peri}$.

No.	Location	Feature
1	T2tumor	log-sigma-1-mm-3D_firstorder_Maximum
2	T2tumor	log-sigma-2-mm-3D_glszm_Large Area Low Gray Level Emphasis
3	T2tumor	log-sigma-4-mm-3D_glszm_Large Area High Gray Level Emphasis
4	T2tumor	wavelet-HHH_first order_Skewness
5	T2tumor	wavelet-HHH_gldm_Small Dependence High Gray Level Emphasis
6	T2tumor	wavelet-LHH_glcm_Correlation
7	T2tumor	wavelet-LHL_glszm_Small Area Emphasis
8	T2tumor	wavelet-LLH_glszm_Size Zone NonUniformity Normalized
9	T2peri	log-sigma-2-mm-3D_glszm_Size Zone NonUniformity Normalized
10	T2peri	original_shape_Maximum 2D Diameter Row
11	T2peri	wavelet-HHL_first order_Skewness
12	T2peri	wavelet-LHH_ngtdm_Busyness
13	T2peri	wavelet-LHL_first order_Median
14	T2peri	wavelet-LLL_ngtdm_Busyness

In the combined model of $T2_{tumor+peri}$, 14 features were selected including 8 $T2_{tumor}$ features and 6 $T2_{peri}$ features, as illustrated in Table 3. In the tumor area, 5 wavelet features and 3 LoG features were identified. In the peritumoral area, the maximum tumor diameter, 4 wavelet features and 1 LoG feature were reserved. All these features reflect the shape, multi-frequency and multi-scale texture information from both the intratumoral and peritumoral tissues.

Radiomics model of $T2_{tumor+peri}$ showed best sensitivity in detecting LNM, and c-LN status showed highest specificity. Thus we proposed a decision tree combining both the Radiomics model of $T2_{tumor+peri}$ and c-LN status for personalized evaluation of LNM, as illustrated in Fig. 3. First, Radiomics model of $T2_{tumor+peri}$ was employed to evaluate if the patients have LNM, if LNM was considered high risk by the model, then we thought LNM was positive for this patient. If LNM was considered as low risk, c-LN status was employed to estimate if LNM did not exist. Patient with c-LN status negative was considered LNM negative and patient with c-LN status positive was considered LNM positive.

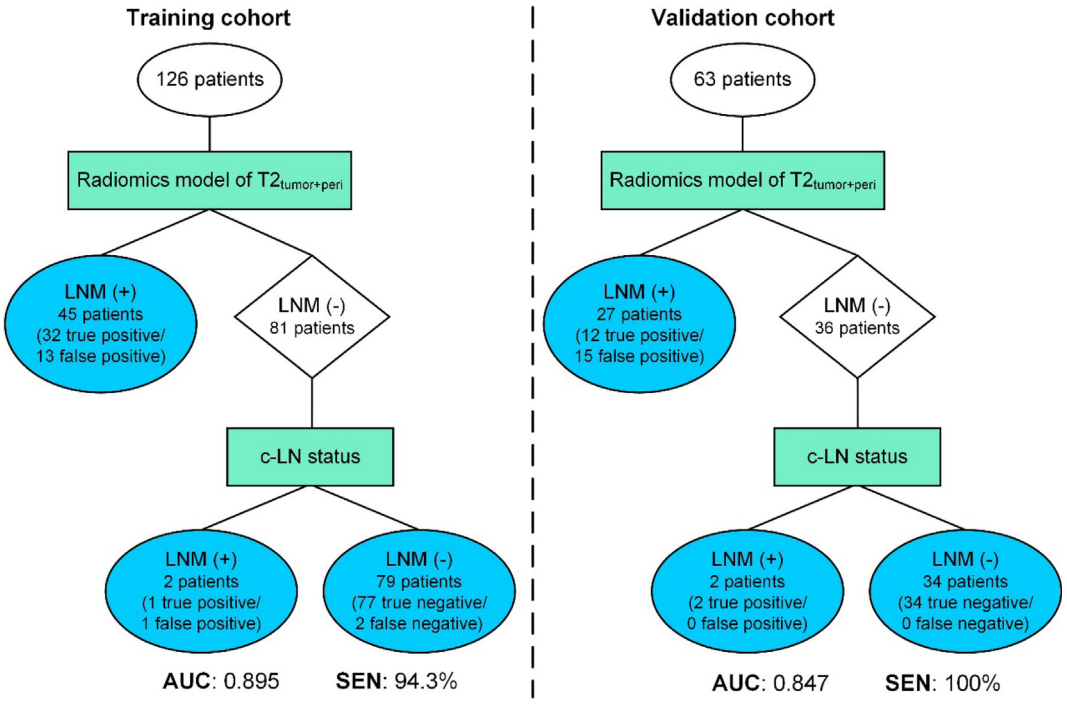

Fig. 3. The decision tree for personalized evaluation of LNM in cervical cancer patients. First, Radiomics model of $T2_{tumor+peri}$ was employed to evaluate if the patients have LNM, if LNM was considered high risk by the model, then we thought LNM was positive for this patient. If LNM was considered as low risk, c-LN status was employed to estimate if LNM did not exist. Patient with c-LN status negative was considered LNM negative and patient with c-LN status positive was considered LNM positive.

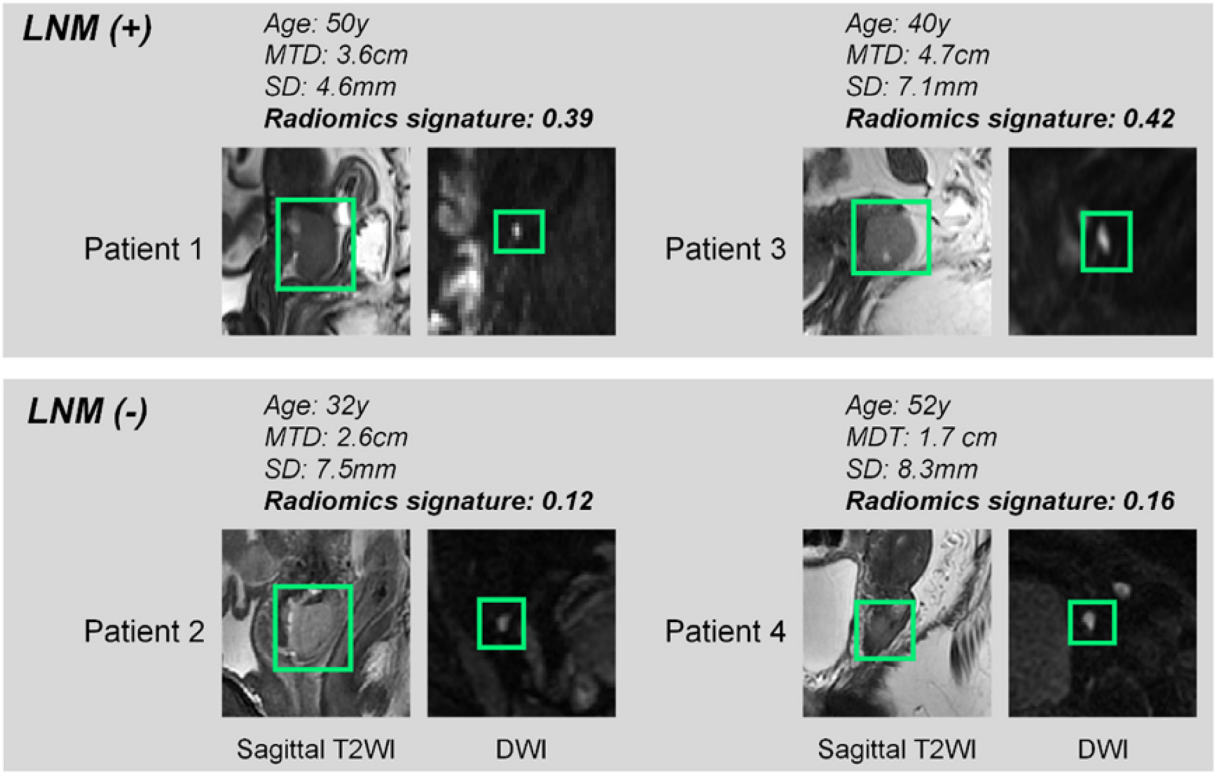

Fig. 4. Representative images. The lesions in the frames on sagittal T2WI are cervical carcinomas and the lesions in the frames on DWI were lymph nodes. Patient 1, a 50-year-old female patient with moderately differentiated squamous cell carcinoma (SCC) and a maximal tumor diameter (MTD) of 3.6 cm, the short diameter (SD) of the largest lymph node (LN) in pelvic area was 4.6 mm. She was classified as high risk for lymph node metastasis (LNM) by radiomics model of $T2_{tumor+peri}$, with radiomics signature of 0.39. This patient turned out to have metastatic LNs histopathologically after surgery. Patient 2, a 32-year-old female patient with poorly differentiated SCC and a MTD of 2.6 cm, and SD of the largest LN was 7.5 mm. She was classified as low risk for LNM by radiomics model of $T2_{tumor+peri}$ and turned out to be LNM negative histopathologically after surgery. Patient 3, a 40-year-old female patient with moderately differentiated SCC with a MTD of 4.7 cm. She was classified as high risk for LNM by radiomics model of $T2_{tumor+peri}$ and turned out to have metastatic LN histopathologically after surgery. Patient 4, a 52-year-old female patient with poorly differentiated SCC with a MTD of 1.7 cm. She was classified as low risk for LNM by radiomics model of $T2_{tumor+peri}$ and turned out to be LNM negative histopathologically after surgery.

The decision tree that combined radiomics model of $T2_{tumor+peri}$ and c-LN status achieved AUC = 0.895, sensitivity = 94.3% and specificity = 84.6% in the training cohort, and AUC = 0.847, sensitivity = 100% and specificity = 69.3% in the validation cohort. Thirty-three out of 35, 14 out of 14 LNM patients in the training and validation cohorts were identified as LNM with the decision tree. Representative images of the personalized evaluation of LNM in four cervical cancer patients were illustrated in Fig. 4.

Discussion

Robust parameters are needed to predict LNM in locally advanced cervical cancer patients in order to select optimal treatment regimen with either surgery or radical chemoradiotherapy. In the present study, we developed a decision tree for personalized preoperative evaluation of LNM in cervical cancer patients. This decision tree incorporates radiomic features of intratumoral and peritumoral tissues on T2WI and c-LN status. Following this decision tree, 94.3% and 100% LNM patients in the training and validation cohorts could be identified and have radical CCRT as their first treatment choice, avoiding surgery and postoperative chemoradiotherapy and more severe complications thereafter. The false negative rate, which equals 1 – sensitivity, should be avoided as much as possible, since the false negative LN status would probably result in the chosen of surgery as the first treatment choice, with the following adjuvant chemoradiotherapy after postoperative pathologically proved LN metastasis. Benefiting from the high sensitivity of the decision tree, positive or suspicious lymph nodes found by the decision tree might direct the gynecologist to convert the treatment plan from surgery to radical chemoradiotherapy. Thirty-two out of 35 patients with LNM in the training cohorts and 14 out of 14 patients with LNM in the validation cohorts were accurately diagnosed as LNM according to the decision tree, meaning that most patients with LNM could be identified and benefit from the decision tree we proposed.

Welch et al. suggested that the radiomics model and clinical factors embedded in the predictive model should be independent because multiple surrogates of the same feature included in the model could impede predictive accuracy [31]. Therefore, we conducted a series of experiments to evaluate the relationship between the radiomics model and multiple clinical factors. The results are shown in the Supplementary Table S1. (1) We evaluated the univariate and multivariate predictive performance of the three relevant preoperative clinical factors (c-LN status, MTD and FIGO stages). As shown in Table 2 and Supplementary Table S1, among the three clinical factors, the performance of identifying LNM is c-LN status > MTD > FIGO, which is consistent with existed studies. In addition, adding MTD and FIGO stages to the c-LN status does not add much additional value since the improvement of adding MTD and FIGO stages is limited especially in the validation cohort. (2) We combined each clinical factor with the radiomics model by decision tree, and assessed the performance of the combined model. We find that combining radiomics model with c-LN status achieves the best performance, indicating that c-LN status contains much complementary information to the radiomics model. (3) We find that adding all the three clinical factors into the decision tree has similar results compared with adding only

c-LN status into the decision tree. Moreover, the decision tree involving only c-LN status gains the best sensitivity. Adding MTD and FIGO stages to the Radi+c-LN model drops the sensitivity. This is probably caused by the following reasons: (a) MTD reflects the tumor size, which is already described by the radiomics model. There is a radiomic feature named "original_shape_Maximum 2D Diameter Row" in Table 3. This radiomic feature reflects the maximum diameter of tumor, which is similar to MTD. Therefore, MTD is a redundant clinical factor to the radiomics model. (b) FIGO stage is a subjective clinical diagnosis whose accuracy is limited, especially in advanced stages [32]. Moreover, FIGO stage in the training cohort does not show significant difference between the LNM positive and LNM negative groups ($p > 0.05$). Therefore, FIGO stage may not bring much discriminative performance. Among the three clinical factors, MTD and FIGO stages are tumor-related features, which may be redundant to the radiomics model since the radiomics model also describes tumor information. However, combining c-LN status with the radiomics model improves the performance because c-LN status is a tumor-independent parameter. Radiomics model reflects tumor information, and c-LN status reflects lymph node information. Therefore, the radiomics model is a complement to c-LN status instead of a surrogate.

Different from previous studies, our study takes the role of radiomic features of peritumoral tissue into account in detecting LNM. In the validation cohort, single layer radiomic features of ADC_{tumor} showed best AUC and sensitivity, which is consistent with our previous study [33]. Radiomic features of peritumoral tissue on ADC maps showed lowest discriminative performance, as we know, the peritumoral tissue displayed as relatively low homogeneous signal intensity (SI) on DWI and high SI on ADC maps, which might provide less useful discriminative information. Thus, when combined radiomic features of intratumoral and peritumoral tissues on ADC maps together, the discriminative efficacy decreased from 0.750 to 0.665. Contrary to ADC maps, the combination of intratumoral and peritumoral tissues on T2WI result in the increase in sensitivity from 64.6% to 85.7%, illustrating that peritumoral tissue of cervical cancer plays an important role in the process of LNM. Heinzelbecker et al. found that lymph vessel density (LVD) in distant normal, peritumor and intratumoral tissues of testicular nonseminomatous germ cell tumors showed significant difference, with intratumoral tissue showing least lymph vessel density, and peritumor LVD was significantly greater in patients with metastasis than those without metastasis [34]. The significantly high specificity from radiomic features of peritumor tissue on T2WI and the improvement of sensitivity when combined intratumoral and peritumoral tissues together support that peritumoral tissue involves and plays an important role in the development of a network of interactions that induce LNM of cervical cancer. Currently, the mostly accepted criterion on MRI in the evaluation of pelvic LNM is the size of the lymph node (c-LN), with the short axis of the LN larger than 1 cm indicating LNM. However, the sensitivity of this criterion is extremely low with 30.3–61.0% reported in the previous studies [8,25], which is in consistent with the sensitivity of 40.1–43.1% in our study. By combining the radiomics model with c-LN status, the decision tree demonstrated high sensitivity in detecting LNM both in the training and validation cohorts, showing a great improvement in the preoperative LNM detection.

A fundamental principle of personalized medicine is to develop therapeutic strategies that address the biological heterogeneity characteristics of cancer [35,36]. Radiomic features extracted from medical imaging can quantify a large panel of phenotypic characteristics which potentially reflect intra- and intertumor heterogeneities [28,37]. The 14 radiomic features enrolled in the model of $T2_{tumor+peri}$ include 8 from intratumoral tissue and 6 from peritumoral tissue. In these features, the MTD was selected automatically, which is consistent with the clinical experience that the tumor size is associated with the LN status, as was shown both in the training and validation cohorts in our study. Moreover, 9 wavelet features and 4 LoG features were included in the radiomics model of $T2_{tumor+peri}$. The wavelet features reflect multi-frequency information of the tumor such as the skewness and texture patterns in various wavelet-transformed frequency range. Similarly, the LoG features extract discriminative texture patterns from multiple space scale. The wavelet and LoG features are extracted from multiple frequency and spatial domain, which are difficult to be visually interpreted in clinical. However, with the quantitative radiomics analysis, these high-dimensional image features are detected and integrated for LN status prediction.

There are some limitations of this study. First, since the radiomics analysis is based on intratumoral and peritumoral tissues, some cervical cancer patients with FIGO stage IB invisible on sagittal T2WI and DWI were excluded, thus the overall prediction value might be underestimated or overestimated. Second, the sample size of patients recruited in this single-centered retrospective study is relatively small that the stratification analysis based on FIGO stage, c-LN status was not done in the validation cohort due to the limited sample size in these subgroups. Larger sample size from multiple centers is needed to confirm the discriminative efficacy of the decision tree we proposed in these subgroups. Third, the LNM prediction is based on patients, rather than LNs, which have limitation in identifying the number and location of metastatic LNs. LN status evaluation based on LNs is needed in the future studies. Fourth, we only used two b values (0 and 800 s/mm^2) in the DWI sequence. Using more and higher low b values (e.g. b values >100 s/mm^2), the discriminative performance of the ADC map may be improved, which is worth our future exploration.

In conclusion, the peritumoral tissue of cervical cancer on T2WI showed favorable value in discriminating LNM. The decision tree, which incorporates radiomic features from intratumoral and peritumoral tissues on T2WI and c-LN status, provides personalized evaluation of LNM with high sensitivity and can be potentially applied in the preoperative prediction of LNM in cervical cancer patients.

Acknowledgement

This study has received funding from National Key R&D Program of China (2017YFE0103600), National Natural Science Foundation of China (81772012, 81720108021), Beijing Natural Science Foundation (7182109), Key Project of Henan Province Medical Science and Technology Project (2018020422); the Youth Innovation Promotion Association CAS (2019136).

Disclosures

The authors indicated no financial relationships.

Appendix A. Supplementary data

Supplementary data to this article can be found online at https://doi.org/10.1016/j.radonc.2019.04.035.

References

[1] Landoni F, Maneo A, Colombo A, Placa F, Milani R, Perego P, et al. Randomised study of radical surgery versus radiotherapy for stage Ib-IIa cervical cancer. Lancet 1997;350:535–40.
[2] Reesink-Peters N, van der Velden J, Ten Hoor KA, Boezen HM, de Vries EG, Schilthuis MS, et al. Preoperative serum squamous cell carcinoma antigen

levels in clinical decision making for patients with early-stage cervical cancer. J Clin Oncol 2005;23:1455–62.
[3] Selman TJ, Mann C, Zamora J, Appleyard TL, Khan K. Diagnostic accuracy of tests for lymph node status in primary cervical cancer: a systematic review and meta-analysis. CMAJ 2008;178:855–62.
[4] Lecuru F, Mathevet P, Querleu D, Leblanc E, Morice P, Darai E, et al. Bilateral negative sentinel nodes accurately predict absence of lymph node metastasis in early cervical cancer: results of the SENTICOL study. J Clin Oncol 2011;29:1686–91.
[5] Cross MJ. Different criteria for radioactive sentinel lymph nodes has different impact on sentinel node biopsy in breast cancer patients. J Surg Oncol 2007;95:616–7.
[6] Sala E, Rockall AG, Freeman SJ, Mitchell DG, Reinhold C. The added role of MR imaging in treatment stratification of patients with gynecologic malignancies: what the radiologist needs to know. Radiology 2013;266:717–40.
[7] Chung HH, Kang KW, Cho JY, Kim JW, Park NH, Song YS, et al. Role of magnetic resonance imaging and positron emission tomography/computed tomography in preoperative lymph node detection of uterine cervical cancer. Am J Obstet Gynecol 2010;203(156):e1–5.
[8] Wu Q, Zheng D, Shi L, Liu M, Wang M, Shi D. Differentiating metastatic from nonmetastatic lymph nodes in cervical cancer patients using monoexponential, biexponential, and stretched exponential diffusion-weighted MR imaging. Eur Radiol 2017;27:5272–9.
[9] Marti-Bonmati L. Lymph node assessment by diffusion weighted imaging in cervical cancer. Eur Radiol 2011;21:474–7.
[10] Kuang F, Ren J, Zhong Q, Liyuan F, Huan Y, Chen Z. The value of apparent diffusion coefficient in the assessment of cervical cancer. Eur Radiol 2013;23:1050–8.
[11] Liu Y, Liu H, Bai X, Ye Z, Sun H, Bai R, et al. Differentiation of metastatic from non-metastatic lymph nodes in patients with uterine cervical cancer using diffusion-weighted imaging. Gynecol Oncol 2011;122:19–24.
[12] Aerts HJ. The potential of radiomic-based phenotyping in precision medicine: a review. JAMA Oncol 2016;2:1636–42.
[13] Liu Z, Wang Y, Liu X, Du Y, Tang Z, Wang K, et al. Radiomics analysis allows for precise prediction of epilepsy in patients with low-grade gliomas. Neuroimage Clin 2018;19:271–8.
[14] Guo J, Liu Z, Shen C, Li Z, Yan F, Tian J, et al. MR-based radiomics signature in differentiating ocular adnexal lymphoma from idiopathic orbital inflammation. Eur Radiol 2018;28:3872–81.
[15] Wang S, Shi J, Ye Z, Dong D, Yu D, Zhou M, et al. Predicting EGFR mutation status in lung adenocarcinoma on CT image using deep learning. Eur Respir J 2019. 1800986.
[16] Huang YQ, Liang CH, He L, Tian J, Liang CS, Chen X, et al. Development and validation of a radiomics nomogram for preoperative prediction of lymph node metastasis in colorectal cancer. J Clin Oncol 2016;34:2157–64.
[17] Wu S, Zheng J, Li Y, Yu H, Shi S, Xie W, et al. A radiomics nomogram for the preoperative prediction of lymph node metastasis in bladder cancer. Clin Cancer Res 2017;23:6904–11.
[18] Dong Y, Feng Q, Yang W, Lu Z, Deng C, Zhang L, et al. Preoperative prediction of sentinel lymph node metastasis in breast cancer based on radiomics of T2-weighted fat-suppression and diffusion-weighted MRI. Eur Radiol 2018;28:582–91.
[19] Shen C, Liu Z, Wang Z, Guo J, Zhang H, Wang Y, et al. Building CT radiomics based nomogram for preoperative esophageal cancer patients lymph node metastasis prediction. Transl Oncol 2018;11:815–24.
[20] Nathanson SD. Insights into the mechanisms of lymph node metastasis. Cancer 2003;98:413–23.
[21] Isaka N, Padera TP, Hagendoorn J, Fukumura D, Jain RK. Peritumor lymphatics induced by vascular endothelial growth factor-C exhibit abnormal function. Cancer Res 2004;64:4400–4.
[22] Padera TP, Kadambi A, di Tomaso E, Carreira CM, Brown EB, Boucher Y, et al. Lymphatic metastasis in the absence of functional intratumor lymphatics. Science 2002;296:1883–6.
[23] Jain RK, Fenton BT. Intratumoral lymphatic vessels: a case of mistaken identity or malfunction? J Natl Cancer Inst 2002;94:417–21.
[24] Jain RK, Tong RT, Munn LL. Effect of vascular normalization by antiangiogenic therapy on interstitial hypertension, peritumor edema, and lymphatic metastasis: insights from a mathematical model. Cancer Res 2007;67:2729–35.
[25] Choi HJ, Roh JW, Seo SS, Lee S, Kim JY, Kim SK, et al. Comparison of the accuracy of magnetic resonance imaging and positron emission tomography/computed tomography in the presurgical detection of lymph node metastases in patients with uterine cervical carcinoma: a prospective study. Cancer 2006;106:914–22.
[26] Braman NM, Etesami M, Prasanna P, Dubchuk C, Gilmore H, Tiwari P, et al. Intratumoral and peritumoral radiomics for the pretreatment prediction of pathological complete response to neoadjuvant chemotherapy based on breast DCE-MRI. Breast Cancer Res 2017;19:57.
[27] Liu Z, Zhang XY, Shi YJ, Wang L, Zhu HT, Tang Z, et al. Radiomics analysis for evaluation of pathological complete response to neoadjuvant chemoradiotherapy in locally advanced rectal cancer. Clin Cancer Res 2017;23:7253–62.
[28] van Griethuysen JJM, Fedorov A, Parmar C, Hosny A, Aucoin N, Narayan V, et al. Computational radiomics system to decode the radiographic phenotype. Cancer Res 2017;77:e104–7.
[29] Rios Velazquez E, Parmar C, Liu Y, Coroller TP, Cruz G, Stringfield O, et al. Somatic mutations drive distinct imaging phenotypes in lung cancer. Cancer Res 2017;77:3922–30.
[30] Shen C, Liu Z, Guan M, Song J, Lian Y, Wang S, et al. 2D and 3D CT radiomics features prognostic performance comparison in non-small cell lung cancer. Transl Oncol 2017;10:886–94.
[31] Welch ML, McIntosh C, Haibe-Kains B, Milosevic MF, Wee L, Dekker A, et al. Vulnerabilities of radiomic signature development: the need for safeguards. Radiother Oncol 2019;130:2–9.
[32] Thomeer MG, Gerestein C, Spronk S, van Doorn HC, van der Ham E, Hunink MG. Clinical examination versus magnetic resonance imaging in the pretreatment staging of cervical carcinoma: systematic review and meta-analysis. Eur Radiol 2013;23:2005–18.
[33] Wu Q, Shi D, Dou S, Shi L, Liu M, Dong L, et al. Radiomics analysis of multiparametric mri evaluates the pathological features of cervical squamous cell carcinoma. J Magn Reson Imaging 2018.
[34] Heinzelbecker J, Gross-Weege M, Weiss C, Horner C, Trunk MJ, Erben P, et al. Microvascular invasion of testicular nonseminomatous germ cell tumors: implications of separate evaluation of lymphatic and blood vessels. J Urol 2014;192:593–9.
[35] Caudell JJ, Torres-Roca JF, Gillies RJ, Enderling H, Kim S, Rishi A, et al. The future of personalised radiotherapy for head and neck cancer. Lancet Oncol 2017;18:e266–73.
[36] Marusyk A, Almendro V, Polyak K. Intra-tumour heterogeneity: a looking glass for cancer? Nat Rev Cancer. 2012;12:323–34.
[37] Wang S, Liu Z, Rong Y, Zhou B, Bai Y, Wei W, et al. Deep learning provides a new computed tomography-based prognostic biomarker for recurrence prediction in high-grade serous ovarian cancer. Radiother Oncol 2019;132:171–7.